

# Flexible Tethered Kite with Moveable Attachment Points, Part I: Dynamics and Control

Paul Williams,\* Bas Lansdorp, Wubbo Ockels  
*Delft University, The Netherlands*

**Tethered kite technology is one potential means of harnessing energy available in high altitude winds. In an efficient and practical system, the kite is required to fly in cyclic patterns that maximize net power produced per cycle. At the same time, the tether length must be controlled to ensure the system does not expend more energy than it produces. This can be a challenging problem when the intermittency of the wind speed and direction, as well as unsteady wind components, are taken into account. This paper is the first of two that studies the dynamics and control of a flexible kite. In this part, a highly simplified dynamic model of the kite is derived based on a hinged, two-plate representation. This first approximation considers aerodynamic forces produced by the plates as a function of their instantaneous angle of attack. The plates are constrained to have the same yawing angle, but are unconstrained in pitch and roll. The combined pitch and roll of the system is controlled by means of moveable attachment points for the tether(s). Both stationkeeping and time-varying trajectories are considered, for which feedback control is applied for tracking.**

## I. Introduction

**T**HE development of kite technology is considered to be an important requirement for future wind power systems, such as the Laddermill.<sup>1-5</sup> The Laddermill is a concept that can enable wind energy to be extracted from higher altitudes than can be reached using conventional systems such as wind turbines. Although there have been many proposals for systems that seek to extract the energy prevalent in the wind at higher altitudes,<sup>6-28</sup> the Laddermill is a concept that has seen much progress in recent years. The advantage of the Laddermill over many other schemes is that the power generation equipment is located on the ground rather than at altitude. This saves a tremendous amount of effort in placing the system at the desired altitude, and also has obvious safety implications. Instead, the system uses a series of light-weight kites attached to a variable length tether. The kites are controlled to produce alternating periods of high and low tension in the tether. This can be achieved by flying the kites in the cross-wind direction and changing the kite angle of attack.<sup>29</sup> A review of high altitude wind power concepts, as well as the development of optimal trajectories for a simplified system are available in Ref. 29. However, in this previous work, the kite dynamics were not explicitly taken into account and it was assumed that the kite angle of attack and roll angle could be controlled. In practice, defining the “kite angle of attack” and “kite roll angle” is nontrivial due to the effects of kite flexibility. This also raises issues related to the implementation of appropriate tracking controllers.

This paper is the first of a two part series. The objective of this series of papers is to focus more attention on certain aspects of kite control. Instead of prescribing the angle of attack and roll angle (which are difficult to define properly for the kite), the actual control actuator that has been implemented is used directly. Two different types of actuators have been considered for remotely piloting kite

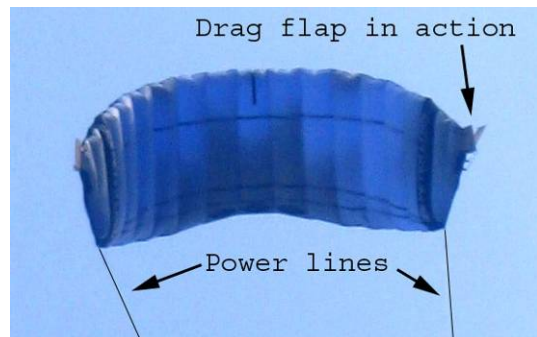


**Fig. 2 Surf-kite with drag flap actuation.**



**Fig. 1 Sliding mechanism along kite edge.**

\* AIAA Member. E-mail: tethered.systems@gmail.com.

systems: 1) extendable drag flaps located on the sides of the kite, and 2) movable attachment points for the tethers. The use of drag flaps for steering (see Fig. 2) has been found to be of limited success in practice due to the relatively poor torque produced by the flaps. Movable attachments are achieved by utilizing a sliding mechanism on the edge of the kite, as shown in Fig. 1. By moving the attachment points, a torque is produced due to the tension in the tether(s), which alters the local angle of attack of the kite. By changing the angle of attack on both sides of the kite, a rolling motion can be produced. The movement of the attachment points is therefore capable of indirectly controlling both the kite angle of attack and its roll angle (more accurately, the tilt of the total lift vector). Hence, this series of papers is aimed at developing a preliminary control strategy for maneuvering the kite by moving the tether attachment points. In this first paper, the dynamics and control of the kite is considered, whereas in the second part, state and wind estimation is considered.

To enable a theoretical and computational study of attachment point control, a mathematical model of the system is required. The main focus here is on the kite control and therefore detailed modeling of the tether(s) is not undertaken. These aspects are presented elsewhere, for example in Ref. 29. Instead, a rudimentary tether model is employed so that coupling between the kite and tether(s) can be simulated. Mathematical modeling of the kite is challenging due to its flexibility. Rather than trying to develop a complex finite element model, a highly simplistic model suitable for preliminary control work is desired. Thus, a multibody model incorporating a hinge joint and two flat kite system. Such a model allows the movement of the tether attachment points to influence each side of the kite, but more importantly, approximates the first mode of the system by allowing each side of the kite to have different pitch and roll angles. This type of model can be extended to consider the kite discretized by multiple plates. A more advanced model is currently being developed, but the details are beyond the scope of this paper.

## II. Simplified Dynamic Model of a Tethered Kite

The kite is modeled as consisting of two flat plates articulated by a frictionless hinge. The basic idea of this approach is that the kite is completely flexible about the centerline in torsion and bending. A real kite is extremely flexible and holds its shape due to aerodynamic forces and tether tension forces. The same idea is used in this model. The plates are hinged at the leading edge for convenience, which would physically allow the plates to collide for particular configurations. However, the model is not intended to be a true representation of the physical structure, but merely an abstract approximation. Hence, collisions are allowed to occur. The tethers are modeled as elastic, but straight. A representation of the model is shown in Fig. 3. The model is considered to be a crude, but realistic representation of the kite system.

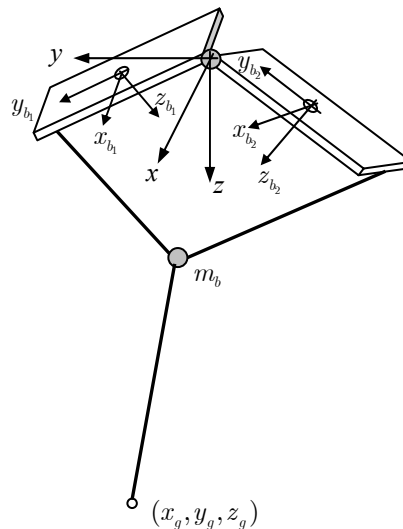
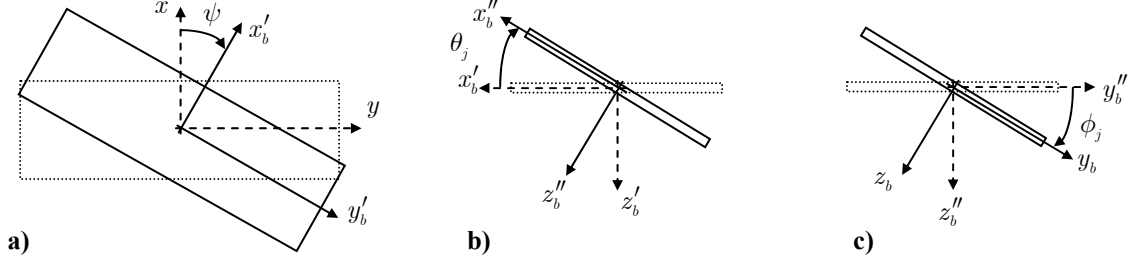


Fig. 3 Simple tethered kite model approximated with two flat plates.

The hinge couples the motion of the two plates through translation as well as rotation. The orientation of each of the plates is specified using the conventional yaw-pitch-roll sequence, shown in Fig. 4. The yaw angles of each

plate are constrained to be the same, since there is little physical ability for the two sides of a real kite to face in different directions. This is due to the presence of tension in the leading and trailing edges that tend to keep the kite straight. The shape of the kite is approximated by allowing the pitch and roll angles of each plate to be different. The actual roll angles of the plates are determined by the positions of the tether attachment points and the aerodynamic forces, as well as the tether tension(s). The pitch of the plates are similarly determined. Because of the coupling between the plates, the equations of motion are derived using Lagrange's equations for simplicity. It can also be noted that it might be possible to construct a semi-rigid version of this abstract model in practice by utilizing a hinge point on the kite.



**Fig. 4 Orientation of plate relative to inertial coordinate system, a) yaw, b) pitch, c) roll.**

The hinge point is used as the reference point for the translational motion of the kite. Its position is defined by the cartesian coordinates  $(x, y, z)$ . The inertial axes are defined such that the  $x$ -axis points predominantly into the direction of the wind, the  $z$ -axis points vertically down, and the  $y$ -axis completes the right-handed triad. Body frames are also used, which are attached to the centers of mass of each plate, as shown in Fig. 3. The positions of the center of mass of the plates relative to the hinge point expressed in the respective body frames can be written as

$$\mathbf{r}_1^{\text{cm}} = -0.5W_1\hat{\mathbf{i}}_1 + 0.5L_1\hat{\mathbf{j}}_1 \quad (1)$$

$$\mathbf{r}_2^{\text{cm}} = -0.5W_2\hat{\mathbf{i}}_2 - 0.5L_2\hat{\mathbf{j}}_2 \quad (2)$$

where the unit vector  $(\hat{\mathbf{i}}_j, \hat{\mathbf{j}}_j, \hat{\mathbf{k}}_j)$  defines the direction of the body axes for plate  $j$ , and  $W_j$  and  $L_j$  are the width and length of the plate  $j$ , respectively. Similarly, the positions of the tether attachment points and aerodynamic centers of the plates relative to the hinge point are expressed as

$$\mathbf{r}_1^{\text{a}} = -u_1W_1\hat{\mathbf{i}}_1 + L_1\hat{\mathbf{j}}_1, \quad \mathbf{r}_2^{\text{a}} = -u_2W_2\hat{\mathbf{i}}_2 - L_2\hat{\mathbf{j}}_2 \quad (3)$$

$$\mathbf{r}_1^{\text{ac}} = -c_aW_1\hat{\mathbf{i}}_1 + l_aL_1\hat{\mathbf{j}}_1, \quad \mathbf{r}_2^{\text{ac}} = -c_aW_2\hat{\mathbf{i}}_2 - l_aL_2\hat{\mathbf{j}}_2 \quad (4)$$

where  $u_j$  is the percentage (fraction) movement of the  $j$ th attachment point from the leading edge of the kite, and  $c_a$  and  $l_a$  are the chordwise and spanwise locations of the aerodynamic center. The chordwise and spanwise locations of the aerodynamic center are assumed fixed in this paper.

The two tethers that are attached to the kite are joined at a bridle, which is modeled as a lumped mass, denoted  $m_b$  in Fig. 3. The complete system of tethers are modeled as extensible springs following Hooke's law. Without loss of generality, the equilibrium position of the kite assumes that the hinge point is located at the origin in the inertial system. In the general configuration, the hinge point is displaced from the origin by the coordinates  $(x, y, z)$ . The position of the mass  $m_b$  is denoted by the coordinates  $\mathbf{R}_b = (x_b, y_b, z_b)$ . Furthermore, denote the position of the main tether on the ground as  $\mathbf{R}_g = (x_g, y_g, z_g)$ . The rationale for including the bridle mass in the model is that it enables all tethers to be modeled as springs. Hence, it is primarily for simplification in the modeling, rather than having a significant practical purpose.

The body frame is related to the inertial frame via the orthogonal transformation

$$C_{I_j}^B = \begin{bmatrix} \cos \theta_j \cos \psi & \cos \theta_j \sin \psi & -\sin \theta_j \\ -\cos \phi_j \sin \psi + \sin \phi_j \sin \theta_j \cos \psi & \cos \phi_j \cos \psi + \sin \phi_j \sin \theta_j \sin \psi & \sin \phi_j \cos \theta_j \\ \sin \phi_j \sin \psi + \cos \phi_j \sin \theta_j \cos \psi & -\sin \phi_j \cos \psi + \cos \phi_j \sin \theta_j \sin \psi & \cos \phi_j \cos \theta_j \end{bmatrix} \quad (5)$$

Hence, the inertial positions of the center of mass, attachment points, and aerodynamic center for each plate are obtained via

$$\mathbf{R}_j^{\text{cm}} = \begin{bmatrix} x \\ y \\ z \end{bmatrix} + [C_{I_j}^B]^T \mathbf{r}_j^{\text{cm}}, \quad \mathbf{R}_j^{\text{a}} = \begin{bmatrix} x \\ y \\ z \end{bmatrix} + [C_{I_j}^B]^T \mathbf{r}_j^{\text{a}}, \quad \mathbf{R}_j^{\text{ac}} = \begin{bmatrix} x \\ y \\ z \end{bmatrix} + [C_{I_j}^B]^T \mathbf{r}_j^{\text{ac}} \quad (6)$$

The velocity of the center of mass of plate  $j$  is given by

$$\begin{aligned} \dot{\mathbf{R}}_j^{\text{cm}} = & [\dot{x} - (\dot{\theta}_j \sin \theta_j \cos \psi + \dot{\psi} \cos \theta_j \sin \psi)X + \{(\sin \phi_j \sin \psi + \cos \phi_j \sin \theta_j \cos \psi)\dot{\phi}_j - (\cos \phi_j \cos \psi + \sin \phi_j \sin \theta_j \sin \psi)\dot{\psi} + \dot{\theta}_j \sin \phi_j \cos \theta_j \cos \psi\}Y, \\ & \dot{y} - (\dot{\theta}_j \sin \theta_j \sin \psi - \dot{\psi} \cos \theta_j \cos \psi)X + \{(-\sin \phi_j \cos \psi + \cos \phi_j \sin \theta_j \sin \psi)\dot{\phi}_j - (\cos \phi_j \sin \psi - \sin \phi_j \sin \theta_j \cos \psi)\dot{\psi} + \dot{\theta}_j \sin \phi_j \cos \theta_j \sin \psi\}Y, \\ & \dot{z} - \dot{\theta}_j X \cos \theta_j + (\dot{\phi}_j \cos \phi_j \cos \theta_j - \dot{\theta}_j \sin \phi_j \sin \theta_j)Y] \end{aligned} \quad (7)$$

where  $X$  and  $Y$  are the components of the vector to the center of mass in the body frame. The kite is assumed symmetrical in the following developments so that  $L_1 = L_2 = L$ ,  $W_1 = W_2 = W$ . The kinetic energy of the kite can be written as

$$T = \frac{1}{2} m_1 \dot{\mathbf{R}}_1^{\text{cm}} \cdot \dot{\mathbf{R}}_1^{\text{cm}} + \frac{1}{2} m_2 \dot{\mathbf{R}}_2^{\text{cm}} \cdot \dot{\mathbf{R}}_2^{\text{cm}} + \frac{1}{2} \boldsymbol{\omega}_1^T [\mathcal{I}] \boldsymbol{\omega}_1 + \frac{1}{2} \boldsymbol{\omega}_2^T [\mathcal{I}] \boldsymbol{\omega}_2 \quad (8)$$

where  $\mathcal{I} = \text{diag}[I_{xx}, I_{yy}, I_{zz}]$  is the inertia matrix of the plate about its center of mass. The angular velocity vector of plate  $j$  is given by

$$\boldsymbol{\omega}_j = [\dot{\phi}_j - \dot{\psi} \sin \theta_j, \dot{\theta}_j \cos \phi_j + \dot{\psi} \cos \theta_j \sin \phi_j, \dot{\psi} \cos \theta_j \cos \phi_j - \dot{\theta}_j \sin \phi_j]^T \quad (9)$$

The effects of tether tension and gravity are incorporated into the generalized forces on the plates rather than via potential energy terms. Thus, the equations of motion for the plates are obtained by applying Lagrange's equations in the form

$$\frac{d}{dt} \left( \frac{\partial T}{\partial \dot{q}_j} \right) - \frac{\partial T}{\partial q_j} = Q_{q_j} \quad (10)$$

The complete equations of motion are too lengthy to be presented here. They are inertially coupled and hence require a matrix inversion for the solution of the second derivatives of the generalized coordinates. The generalized forces are also quite complex due to the coupling between translations and rotations. However, the actual forces applied to the kite, expressed in the inertial frame, are relatively simple. The important forces acting on the plates are the aerodynamic forces, gravity forces, and tether tension forces. These are derived in the following subsections.

### A. Aerodynamic Forces

As a first approximation, the aerodynamic forces are computed by using the relative wind velocity at the center of the plate. Thus, the lift and drag coefficients are based on the relative wind velocity at a single point on each side of the kite. The total lift and drag forces are applied at the aerodynamic center of the plate. The relative inertial wind speed at the center of the plate is obtained as

$$\mathbf{V}_j^{\text{rel}} = \dot{\mathbf{R}}_j^{\text{cm}} - \mathbf{V}_{\text{wind}} \quad (11)$$

Using Eq. (5), the components of the relative wind in the body frame of the plate are obtained as

$$\mathbf{v}_j^{\text{rel}} = [C_{I_j}^B] \mathbf{V}_j^{\text{rel}} \quad (12)$$

The angle of attack and sideslip angles are

$$\alpha_j = \tan^{-1} \left( \frac{\mathbf{v}_j^{\text{rel}} \cdot \mathbf{k}_j}{\mathbf{v}_j^{\text{rel}} \cdot \mathbf{i}_j} \right), \quad \beta_j = \sin^{-1} \left( \frac{\mathbf{v}_j^{\text{rel}} \cdot \mathbf{j}_j}{|\mathbf{v}_j^{\text{rel}}|} \right) \quad (13)$$

with the plate dynamic pressures defined by

$$\bar{q}_j = \frac{1}{2} \rho_j |\mathbf{v}_j^{\text{rel}}|^2 \quad (14)$$

The lift and drag coefficients of the plates are approximated via the following common expressions

$$C_{L_j} = C_{L_0} \alpha_j, \quad C_{D_j} = C_{D_0} + kC_{L_j}^2, \quad \alpha \leq \alpha_{\max} \quad (15)$$

Alternatively, lookup tables of experimentally derived force coefficients can be used. Pure flat plate lift and drag coefficients are not used because the kite is a finite wing. The body force coefficients can be related to the lift and drag coefficients via a simple rotation by the angle of attack as follows

$$\begin{aligned} C_{X_j} &= -C_{D_j} \cos \alpha_j + C_{L_j} \sin \alpha_j \\ C_{Z_j} &= -C_{D_j} \sin \alpha_j - C_{L_j} \cos \alpha_j \end{aligned} \quad (16)$$

From these definitions, the body forces are obtained in the standard way

$$F_{X_j} = C_{X_j} \bar{q}_j S_j, \quad F_{Y_j} = C_{Y_j} \bar{q}_j S_j, \quad F_{Z_j} = C_{Z_j} \bar{q}_j S_j \quad (17)$$

where  $S_j$  is the plate area. Finally, the aerodynamic forces applied in the inertial frame are given by the vector

$$\mathbf{F}_j^{\text{aero}} = [C_{L_j}^B]^T [F_{X_j}, F_{Y_j}, F_{Z_j}]^T \quad (18)$$

Note that these forces are applied at the aerodynamic center of each plate, whose position is defined by  $\mathbf{R}_j^{\text{ac}}$  in Eq. (6). This is only of relevance to the computation of the moments on the plates. The generalized forces appearing in Eq. (10) due to aerodynamic effects are computed as

$$Q_{q_j}^{\text{aero}} = \mathbf{F}_j^{\text{aero}} \cdot \frac{\partial \mathbf{R}_j^{\text{ac}}}{\partial q_j}, \quad i = 1, 2 \quad (19)$$

Simple aerodynamic damping moments are also applied to each plate in the form

$$Q_{\theta_j} = C_{m_\theta} \dot{\theta}_j \bar{q}_j S_j W_j, \quad Q_{\phi_j} = C_{m_\phi} \dot{\phi}_j \bar{q}_j S_j W_j \quad (20)$$

The aerodynamic moments provide damping to the kite because of the relatively large ratio of air mass to kite mass for most kite systems. It must also be noted that side forces, and unsteady forces have been neglected in this model, but can be added relatively easily when these are known. These forces are likely to be extremely important. However, system identification procedures using experimental data must be performed to derive an adequate representation of them. This is also an avenue of research that is currently being pursued vigorously. However, for the time being, simple lift, drag, and damping forces are used in the model.

## B. Gravity Forces

Gravitational forces are applied at the center of the plates according to

$$\mathbf{F}_j^g = [0, 0, m_j g]^T \quad (21)$$

The generalized forces are calculated via

$$Q_{q_j}^g = \mathbf{F}_j^g \cdot \frac{\partial \mathbf{R}_j^{\text{cm}}}{\partial q_j}, \quad i = 1, 2 \quad (22)$$

## C. Tension Forces

The tension forces acting on the plates give rise to both applied forces and moments. The moments are particularly important because control of the system is sought by moving the positions of the tether attachment points on the kite. Here, the pitch and roll of the plates can be indirectly controlled by moving the attachment point in the appropriate manner. This is challenging, in light of the limited movement that is available. We will begin by first defining the equations of motion of the bridle mass. For simplicity, we have ignored aerodynamic forces on the mass and will only treat tension and gravity forces. Thus,

$$m_b \ddot{\mathbf{R}}_b = \mathbf{T}_3 - \mathbf{T}_1 - \mathbf{T}_2 + m_b g \mathbf{k} \quad (23)$$

The directions of the tension force vectors are defined in Fig. 5. The tensions acting on the attachment points of the kite can be defined by

$$\mathbf{T}_j = \frac{EA}{L_{s_j}} \left( |\mathbf{R}_b - \mathbf{R}_j^a| - L_{s_j} \right) \frac{\mathbf{R}_b - \mathbf{R}_j^a}{|\mathbf{R}_b - \mathbf{R}_j^a|}, \quad j = 1, 2 \quad (24)$$

where  $EA$  is the longitudinal stiffness of the tether, and  $L_{s_j}$  is the unstrained length of the  $j$ th tether.

The tension vector from the main tether line is defined by

$$\mathbf{T}_3 = \frac{EA}{L_{s_3}} \left( \|\mathbf{R}_g - \mathbf{R}_b\| - L_{s_3} \right) \frac{\mathbf{R}_g - \mathbf{R}_b}{\|\mathbf{R}_g - \mathbf{R}_b\|} \quad (25)$$

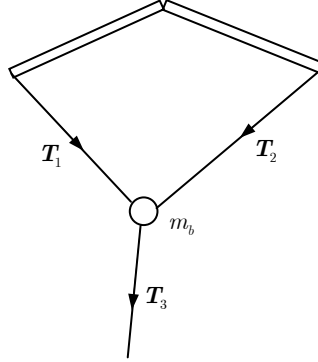


**Fig. 5 Tension vector definition for bridle mass equations of motion.**

Hence, by specifying the time evolution of the position of the attachment points, and with knowledge of the current position of the bridle mass, the tension vectors are determined. The tension forces acting on the kite give rise to pitch and roll moments, which are accounted for in the kite dynamics by the following generalized forces

$$Q_{q_j}^{\text{tension}} = \mathbf{T}_1 \cdot \frac{\partial \mathbf{R}_1^a}{\partial \mathbf{q}_j} + \mathbf{T}_2 \cdot \frac{\partial \mathbf{R}_2^a}{\partial \mathbf{q}_j} \quad (26)$$

The entire set of equations of motion are constructed in state-space form and numerically integrated using a variable-step stiff integration routine.

### III. Equilibrium Configuration for Stationkeeping

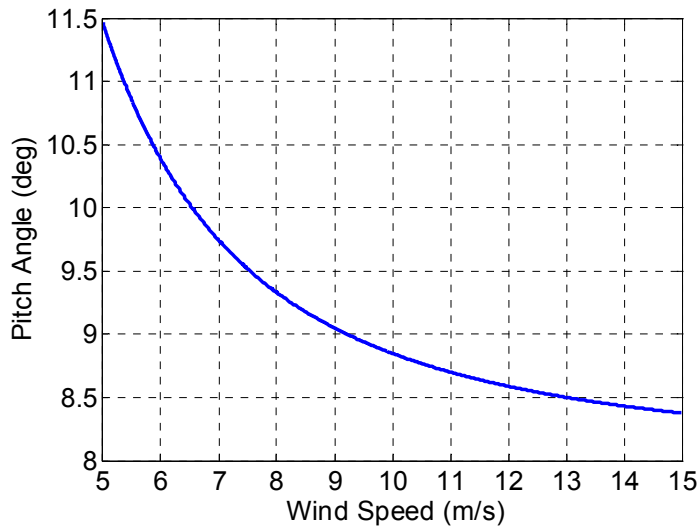
One of the features of kite-flying, as well as the mathematical model presented in the previous section, is that it can be difficult to establish an equilibrium configuration. In practice, the difficulty can be that the wind speed is unsteady, whereas in the mathematical model, the challenge is to find a configuration that gives the correct balance between lift/drag forces, gravity, and tether tension. In this paper, equilibrium configurations are determined as a function of the wind speed by specifying the coordinates of the hinge point and treating the yaw, pitch, and roll angles of the plates as unknowns. The unstrained lengths of the tethers are specified, and the position of the bridle mass is determined to ensure that the system is not accelerating. As mentioned previously, the equations of motion are highly nonlinear and extremely complicated. Hence, analytic solutions for equilibria are not possible in general. The position of the tether at the ground is a function of the length of tether 3. It does not alter the equilibria of the kite in any way and hence is only incorporated once a solution has been obtained. The equilibrium configurations are solved using the solver SNOPT<sup>30</sup> with finite differences used to approximate the Jacobians.

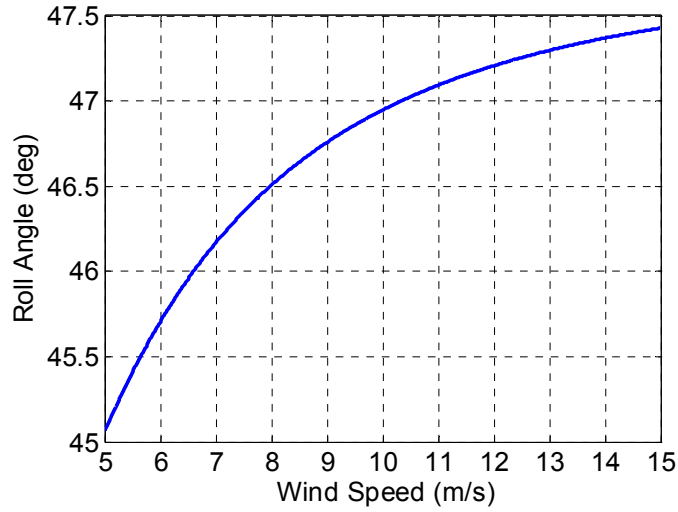
The unknowns that feature in the equilibrium problem are the yaw, pitch and roll of the plates, the position of the bridle, and the position of the attachment points. Symmetry is enforced so that the pitch of both plates are equal (in addition to the yaw), and that the roll angles are antisymmetric. However, this still does not give a unique solution. Various combinations of attachment point positions were found to give different equilibrium positions. To make the equilibrium solutions unique, we seek to drive the attachment point to the quarter chord position. This is somewhat arbitrary, because in this paper the primary goal is to keep the kite close to the zenith position. In practice, one might want to position the attachment points such that the maximum lift/drag ratio is obtained. Thus, all of the results in the following are for the attachment points at quarter chord. The nominal system parameters used to compute equilibria are given in Table 1.

**Table 1 Nominal system parameters.**

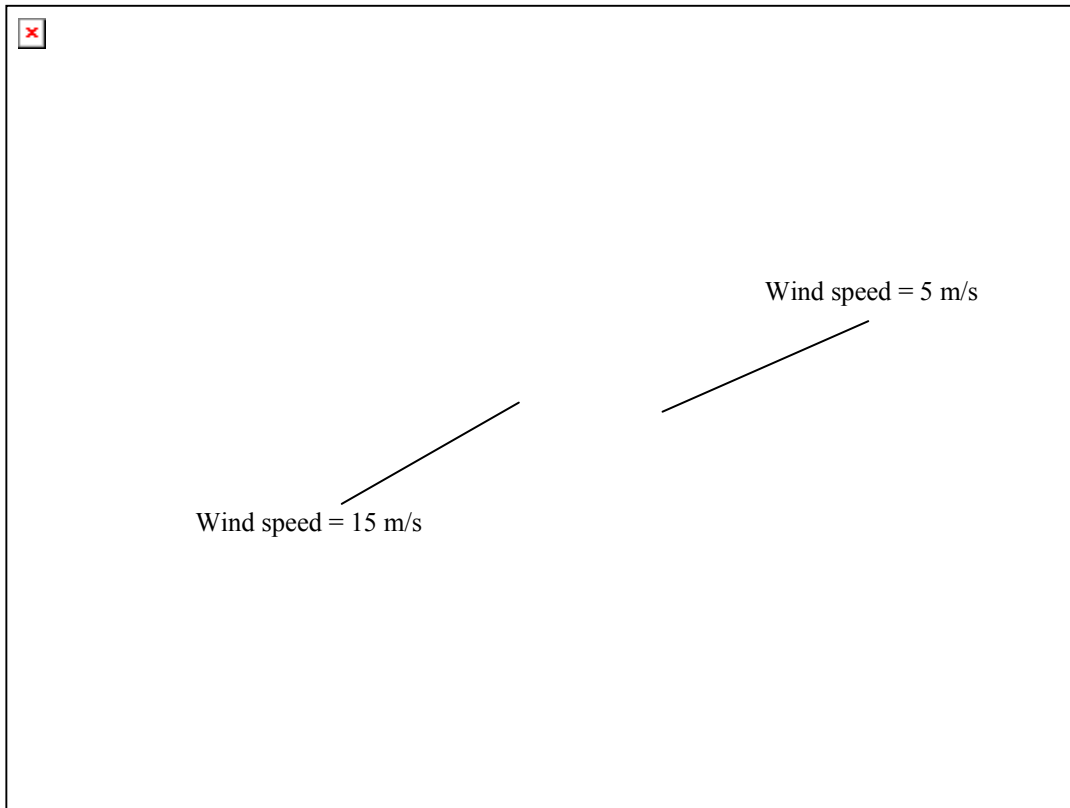
Parameter	Value
Plate width, $W$	0.5 m
Plate length, $L$	3 m
Plate mass, $m$	0.25 kg
Chordwise location of a.c.	30 %
Spanwise location of a.c.	50 %
Air density	1.225 kg/m <sup>3</sup>
$C_{L_0}$	6 /rad
$C_{D_0}$	0.03
$k$	0.1
Bridle mass, $m_b$	0.1 kg
Length of grounding tether	300 m
Tether stiffness, $EA$	10000 N
Length of bridle tethers	20 m

Fig. 6 shows the equilibrium pitch angle of the plates as a function of the wind speed, which is assumed to be parallel to the  $x$ -axis. As might be expected, for low wind speeds, the pitch angle must be large to generate a sufficient angle of attack to support the system. As the wind speed increases, the pitch angle decreases nearly quadratically (although it is also a function of the roll angle and magnitude of the tether tension). Fig. 7 shows the roll angle of the plates (note that one plate has a negative roll angle) as a function of the wind speed. This illustrates that the roll angle increases as the wind speed increases, although the change is only on the order of two degrees. The change in the roll angle affects the direction of the lift forces on the plates. Because the attachment point position remains fixed, the kite must reorient itself to ensure that the moments generated by the tethers are balanced properly. Fig. 8 shows a scale plot of the plate and tether equilibrium positions as a function of wind speed. This shows that the system orientation becomes more vertical as the wind speed increases. This result depends on the break-up of the lift and drag forces. Typically, the higher angle of attack configuration generates larger drag coefficients, and the influence of kite mass decreases compared to the aerodynamic forces at high wind. For low wind speeds, a larger angle to the vertical is required to adequately balance the moments on the plates.

**Fig. 6 Plate pitch angle vs. wind speed with attachment points at the quarter chord position.**



**Fig. 7 Plate roll angle vs. wind speed with attachment points at the quarter chord position.**



**Fig. 8 Kite model and tether equilibrium positions for various wind speeds.**

A stability analysis of the open-loop system reveals, intuitively, that the system is unstable. That is, any disturbance of the system away from equilibrium will cause the system to diverge unless some kind of active control is used. For this reason, we first investigate the possibility of stabilizing the system automatically by moving the tether attachment points based on feedback of the system dynamic states.

## A. Stationkeeping Control

In this subsection, the capability of maintaining the desired position and orientation of the kite is considered using state feedback. Here, full state feedback is assumed. The dynamics of the kite will be difficult to measure directly, and hence, some form of estimator must be developed. This is considered in Part II of this paper series. Although nonlinear controllers would be possible for stabilizing the kite, only a linear feedback controller is considered here for simplicity. A linear receding horizon strategy is used to develop the feedback control gains for the system. Such an approach reduces to a linear quadratic regulator (LQR) for infinite horizon problems. In the general case, the tracking controller needs to be capable of tracking the time-varying reference trajectories that produce maximum power output. Although some energy must be expended in actuating the kite, we do not focus on this cost. In the optimal control formulation, however, the variation in the control inputs is minimized, but this is done here to achieve stability rather than a desire to limit actuation energy. Future work will necessitate calculating the energy required to implement the control actuators.

### 1. Control Gains For General Time-Varying Trajectories

One of the challenges with using a kite-type system for extracting wind energy is that it is likely to be sensitive to gusts and turbulence. In other words, variations in the wind speed could disturb the system significantly, causing it to enter into an unrecoverable spin, dive, or collapse. Later, time-varying trajectories will be developed for the system, and it is necessary for the feedback controller to track these more general trajectories. Stationkeeping can be considered as a simplified tracking control problem. The control gains used to implement the feedback control are determined by solving the following optimization problem in state-space form: find the controls  $\delta \mathbf{u}(t)$  that minimize the quadratic performance index

$$\delta J = \frac{1}{2} \delta \mathbf{x}^\top(t + T_h) \mathbf{S}_f \delta \mathbf{x}(t + T_h) + \frac{1}{2} \int_t^{t+T_h} [\delta \mathbf{x}^\top(t) \mathbf{Q} \delta \mathbf{x}(t) + \delta \mathbf{u}^\top(t) \mathbf{R} \delta \mathbf{u}(t)] dt^* \quad (27)$$

subject to the linearized state equations

$$\delta \dot{\mathbf{x}} = \mathbf{A}(t) \delta \mathbf{x} + \mathbf{B}(t) \delta \mathbf{u} \quad (28)$$

the initial conditions

$$\delta \mathbf{x}(t^* = t) = \mathbf{x}(t) - \bar{\mathbf{x}}(t) \quad (29)$$

and possibly the terminal constraints

$$\delta \mathbf{x}(t^* = t + T_h) = 0 \quad (30)$$

where  $\delta \mathbf{x} \in \mathbb{R}^{n_x}$  are the perturbed state variables,  $\delta \mathbf{u} \in \mathbb{R}^{n_u}$  are the perturbed controls,  $\mathbf{A} \in \mathbb{R}^{n_x \times n_x}$  is the time-varying system state influence matrix,  $\mathbf{B} \in \mathbb{R}^{n_x \times n_u}$  is the time-varying control influence matrix,  $\mathbf{Q} \in \mathbb{R}^{n_x \times n_x}$  is a positive semi-definite weighting matrix that penalizes the deviations of the perturbed states,  $\mathbf{R} \in \mathbb{R}^{n_u \times n_u}$  is a positive definite weight matrix that penalizes the deviations of the perturbed controls, and  $\mathbf{S}_f \in \mathbb{R}^{n_x \times n_x}$  is a positive semi-definite terminal weight matrix that penalizes the deviations of the perturbed states at the end of the future horizon  $T_h$ .

The solution of the above optimization problem is obtained using a Gauss-Lobatto<sup>31</sup> or Legendre pseudospectral discretization<sup>32</sup> combined with standard results from quadratic programming. The final result is a feedback controller of the form

$$\delta \mathbf{u}(t) \triangleq \mathbf{K}(t; N, T_h) \delta \mathbf{x}(t) \quad (31)$$

The control gains are stored along with the reference trajectory and must be interpolated during implementation. In the case of stationkeeping control, the control gains and reference trajectory are fixed.

### 2. Simulations with Unsteady Winds

To conduct a full simulation, the grounding tether must be incorporated into the system and equilibria. The grounding tether is selected to be 300 m long, so the scale of the system is much reduced from the large-scale wind power production systems envisaged in Refs. 3-5. In the following results, the weighting matrices were selected as:  $\mathbf{Q} = \text{diag}[5, 5, 5, 1, 5, 5, 5, 5, 1, 1, 1, 1, 1, 1, 1, 1, 1, 1, 1, 1]$ ,  $\mathbf{R} = \text{diag}[200, 200]$ , where the state vector is defined as

$$\mathbf{x} \triangleq [x, y, z, \psi, \theta_1, \phi_1, \theta_2, \phi_2, x_b, y_b, z_b, \dot{x}, \dot{y}, \dot{z}, \dot{\psi}, \dot{\theta}_1, \dot{\phi}_1, \dot{\theta}_2, \dot{\phi}_2, \dot{x}_b, \dot{y}_b, \dot{z}_b] \quad (32)$$

The rationale for these choices is that the position of the kite should be kept as close to the zenith as possible, with penalties on the variation of the pitch and roll angles. All other state variables are weighted equally. The control penalty is selected to be large enough to limit the movement of the attachment points. Saturation of the attachment points causes a loss of full control authority assumed in the calculation of the feedback gains, which can cause the system to become unstable. Future controllers will need to consider constrained feedback control to fully exploit the system's capabilities.

The following results are for a nominal wind speed of 5 m/s, with white-noise fluctuations superimposed in the  $x$ - and  $y$ -directions. Numerical results from a 5-minute simulation are shown in Fig. 9. Fig. 9a shows the components of the unsteady wind. The cross-wind components have larger variations than the wind component parallel to the nominal wind direction. This can be interpreted as a wind that changes in magnitude and direction as a function of time. Using this interpretation, the wind speed fluctuates by up to 1 m/s and the direction fluctuates by up to 30 deg. Throughout this paper, the mean of any perturbations is assumed to be zero, so that the controller remains valid. Changes in the mean wind speed would at least require an integrator to compensate for steady-state errors. The results for the position control are shown in Fig. 9b, which gives the hinge point position as a function of time. It can be seen that the  $x$ - and  $z$ - positions of the hinge have both low and high frequency components as a result of the disturbances. The high frequency components are due to the high frequency changes in the wind speeds. The  $y$ -position of the hinge is dominated by the changes in the cross-wind speed, or wind direction. It can be seen from Fig. 9b that the position of the kite is maintained extremely well by movement of the attachments, with the maximum Euclidean error peaking at 3.5 m and a mean of approximately 1.0 m. The yaw angle of the kite is shown in Fig. 9c, which illustrates fluctuations of up to 25 deg. The pitch angles of the plates, shown in Fig. 9d, vary by approximately  $\pm 8$  deg from the nominal. In addition, the results clearly show that the pitch of the two plates are slightly different. The roll angle on the other hand, shown in Fig. 9e, shows that the kite maintains close symmetry around the  $y$ -axis, although some asymmetry is required in order to maintain the hinge point at the desired location. Note that because one roll angle is the negative of the other, the result is mirrored around the mean value. The symmetry can be seen by examining the peaks of the roll angle for each plate. Finally, the attachment point position as a fraction of the chord is given in Fig. 9f. The mean movement of the attachment is approximately 5 % from the equilibrium position. The maximum movement of the attachments is on the order of 25% of the chord, where attachment 2 saturates at the lower bound. Because the nominal attachment point position is 0.25, the lower bound of 0 is the critical one. Larger disturbances can cause saturation, which obviously limits the effectiveness of the actuator. If it is found that such saturation is critical, it might be necessary to incorporate additional control actuators, such as the drag flaps discussed in the Introduction. However, this adds more cost to the system, as well as complexity and cost.

## **B. Classical PID Control for Small-Scale Test Kite**

In the previous section, a controller based on full state feedback was implemented under the assumption that the kite model can be refined enough to be representative of a real system. In this section, an additional controller that will be used in initial testing of the kite is presented based on classical PID control. Although this controller is tuned based on the two-plate model, it does not assume full state feedback, and should be capable of being tuned to the real kite during operation. The objective of the kite is to maintain the kite as close to the zenith as possible. The only measurements that are assumed to be available are the kite position (hinge point), and mean pitch angle of the kite. Here, the mean pitch angle is taken as the average pitch of the two plates. The structure of the controller is shown in Fig. 10. The controller is implemented as a discrete time controller running at a sampling frequency of 100 Hz. The motion of each attachment point is controlled based on symmetric and antisymmetric demands. Symmetric demands are used to control the kite altitude and pitch angle, whereas antisymmetric demands are used for controlling the lateral kite position. The kite lateral position is controlled using the lateral position of the hinge point and its velocity. Steady-state errors in height and lateral position are handled using trapezoidal integrators. Furthermore, for better stability, a PI controller for the mean kite pitch angle is also used. The feedback control is combined with a feedforward control term, which in this case is the trim position of the attachments.

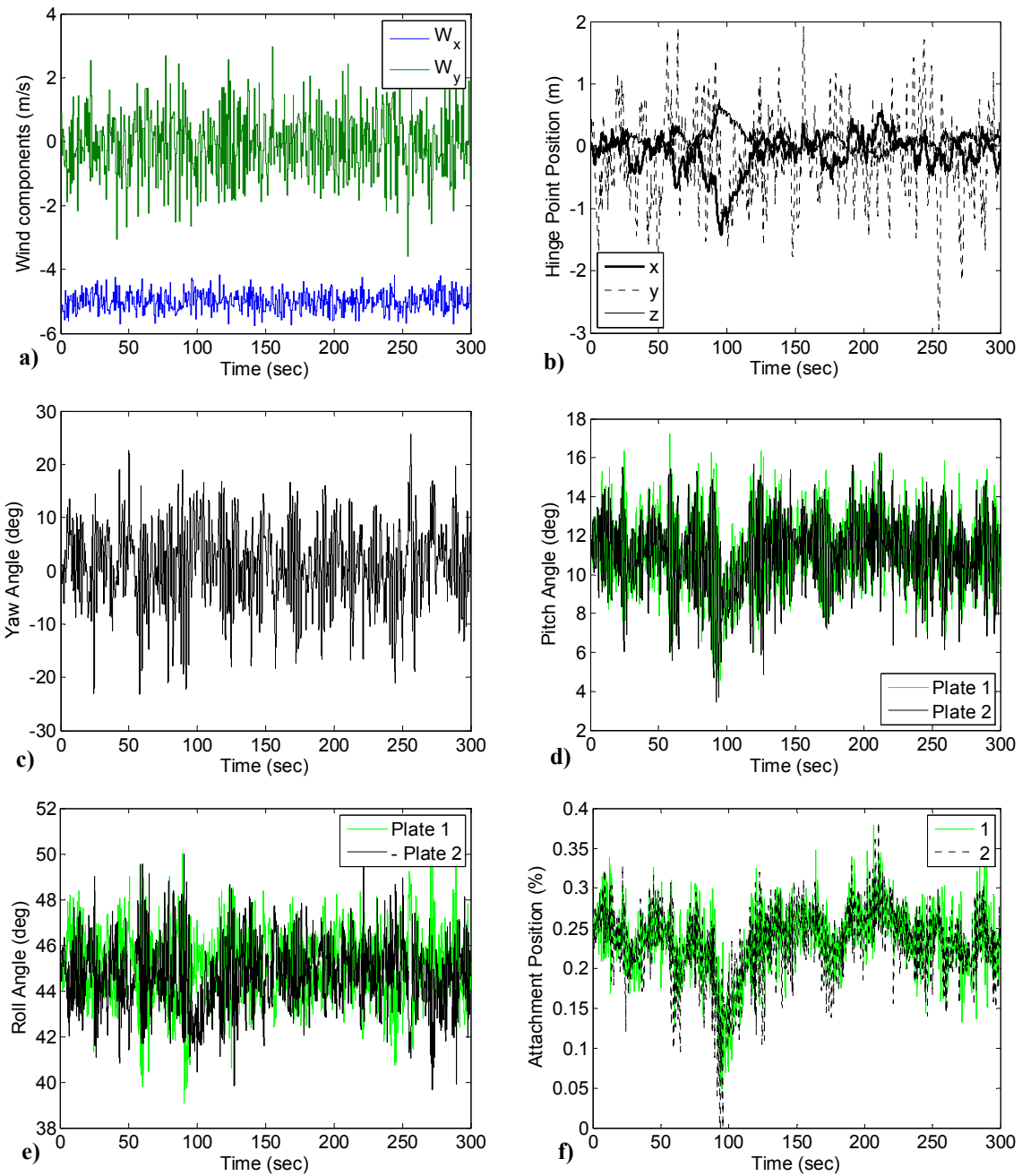


**Fig. 9 Stationkeeping simulation results with unsteady winds, a) Wind time history, b) Hinge point position, c) Kite yaw angle, d) Pitch angle of plates, e) Roll angle of plates (plate 2 is shown as negative roll angle), f) Attachment point position as fraction of chord.**

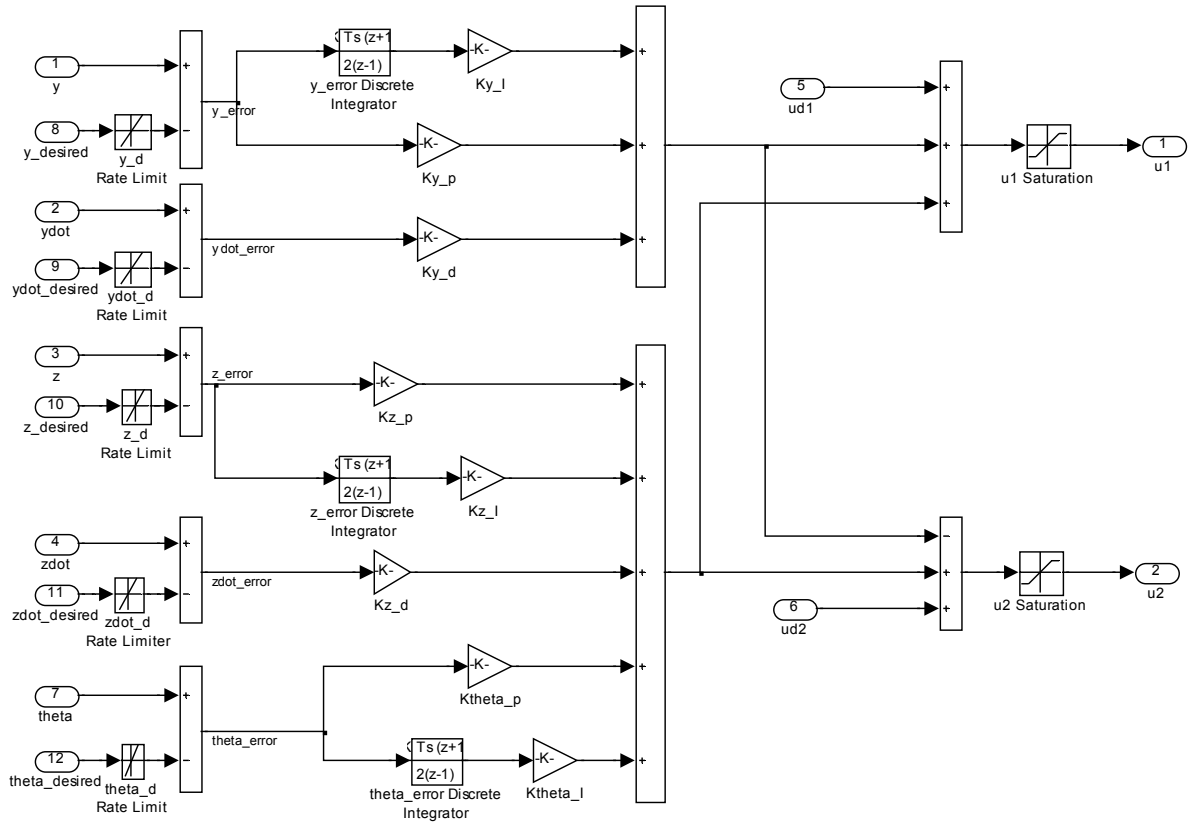


**Fig. 10 Control block-diagram for kite PID control.**

The small-scale test system consists of the same size kite shown in Table 1, but the grounding tether is 30 m long, and the bridle tethers are both 5 m long. The controller is simulated with a demanded step input of  $y = 1$  m after 200 sec. Results are shown in Fig. 11 for a 500 sec simulation. The results show that the kite position is maintained to within approximately 20 cm in downwind position, 10 cm in height, and approximately 2 cm errors in lateral position for the given wind perturbations. The lateral position error increases slightly at the time of the step input, but it is clear that the controller adequately stabilizes the kite in the unsteady wind. The effect of an asymmetric position demand can be seen in the response of the plate roll angles. The mean difference in roll angles is on the order of 5 deg after 200 sec. Prior to this, the roll angles share a similar mean and are generally symmetric. Fig. 11f shows that the lateral position offset is achieved with a mean difference in attachment point positions of 1.5 %.

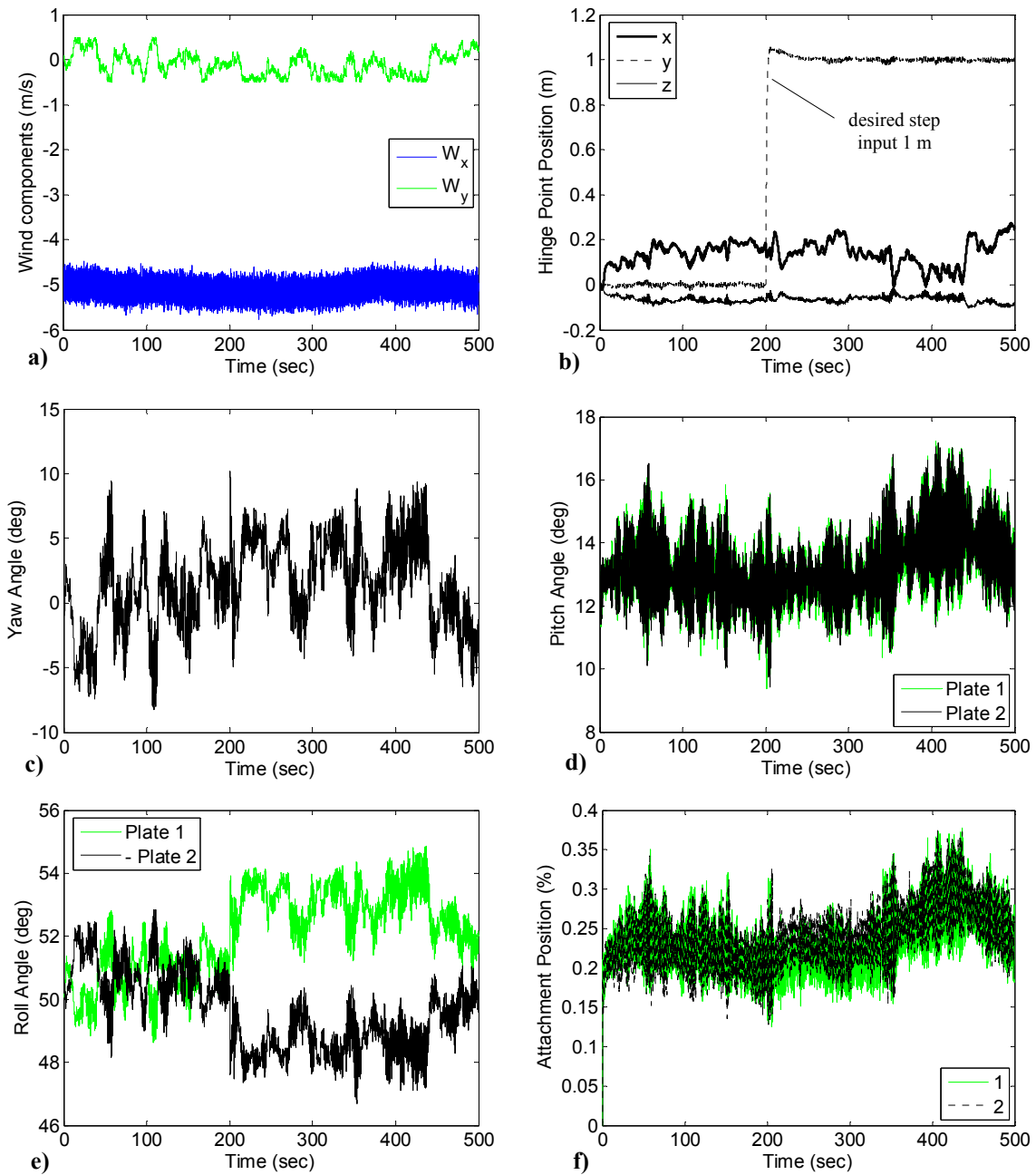


**Fig. 11** Simulation results of PID controller with unsteady winds, a) Wind time history, b) Hinge point position, c) Kite yaw angle, d) Pitch angle of plates, e) Roll angle of plates (plate 2 is shown as negative roll angle), f) Attachment point position as fraction of chord.

## IV. Optimal Maneuvering Control

Stationkeeping control is a relatively simple problem if the kite equilibrium configuration is known and the system states can be measured. A more difficult problem involves trying to maneuver the kite along, or near, desired trajectories. This is more difficult because first a set of suitable reference trajectories need to be generated. The reference trajectories should satisfy some particular requirements for the system, but should also enable efficient tracking. For example, if the reference control actuator input is bang-bang, then this would be extremely difficult to track due to system uncertainties and disturbances. One way around this is to use conservative constraints on the actuator inputs to allow room for uncertainties. Another way is to incorporate some measure of tracking ability into the system design.

Ultimately, the kite is desired to move along trajectories that maximize the power generated by a ground station.<sup>29</sup> A preliminary analysis of optimal trajectories for power generation is presented in Ref. 29, which employed a simple point mass model of the kite controlled via angle of attack and roll angle (tilt of the lift vector). The means for generating optimal power is a very important problem, but this is not the focus of the current paper. Instead, we will generate arbitrary time-varying periodic trajectories for the system. We will then attempt to track these trajectories using the state-space tracking controller described in the previous section. To deal with the issue of tracking ability, we treat the control inputs into the system as the attachment point velocities rather than the attachment point positions. We then utilize an optimal control algorithm to minimize a weighted cost that includes the  $L_2$ -norm of the attachment point velocities. The rationale for this is that the optimal control input in such a case is continuous, smooth, and one of minimal variation. This implies a smooth variation in attachment point position and should improve the trackability of the reference trajectories.

### A. Trajectory Generation Method

To generate trajectories that move close to a prescribed path, a nonlinear optimal control problem is solved. The basic problem is posed as follows: Find the time history of the attachment point velocities  $\mathbf{u}(t)$  that minimize the cost

$$J = \int_{t_0}^{t_0+T} \left[ W_1 (x_h - \bar{x}_h)^2 + W_2 (y_h - \bar{y}_h)^2 + W_3 (z_h - \bar{z}_h)^2 + u_1^2 + u_2^2 \right] dt \quad (33)$$

subject to the dynamic constraints

$$\dot{\mathbf{x}} = \mathbf{f}(\mathbf{x}(t), \mathbf{u}(t), t) \quad (34)$$

where  $\mathbf{f}(\mathbf{x}(t), \mathbf{u}(t), t)$  are the equations of motion of the kite, and the subscript  $h$  in Eq. (33) represents the hinge point position. The overbars in (33) denote an idealized reference path for the variables. The following periodicity constraints are also enforced

$$\mathbf{x}(t_0) = \mathbf{x}(t_0 + T) \quad (35)$$

The position of the attachment points are obtained by integrating the rates,  $\dot{\mathbf{x}}_a = \mathbf{u}$ . Both the positions and the rates are subject to inequality constraints

$$0 \leq x_a(t) \leq 1, \quad \mathbf{u}_{\min} \leq \mathbf{u}(t) \leq \mathbf{u}_{\max} \quad (36)$$

The above optimal control problem basically trades the error of the kite from the idealised reference path with the control variation required to achieve it. The coefficients  $W_j, j = 1, 2, 3$  provide a means for weighting particular requirements. For example, cross-wind motion may take precedence over vertical or downwind motion, in which case  $W_2$  would be set to a high value and  $W_1$  and  $W_3$  would be set small. The weighting terms should also be scaled relative to the desired penalty to be placed on the actuator inputs, since the absolute value of the cost is not important (although it makes a difference in numerical computations due to scaling). The optimal control problem is solved numerically using the Legendre pseudospectral method described in the following section.

### B. Numerical Method

The optimal control problem defined in the preceding subsections is solved using the Legendre pseudospectral method.<sup>33,34</sup> Essentially, this approach discretizes the states and controls using Lagrange interpolating polynomials expanded at the Legendre-Gauss-Lobatto points for a specified order- $N$  polynomial. The consequence of this choice is that the optimization parameters are the values of the states and controls themselves, as opposed to polynomial coefficients that usually do not have a physical meaning. In addition, the cost function is easily discretized by means of Gauss-Lobatto quadrature. The state equations are enforced in an approximate fashion by differentiating

the interpolating polynomials for the states and employing an equality constraint at each LGL point. The equality constraints require the state derivatives to be equal to the vector field at the corresponding LGL point. Mathematical details are given in the following subsection.

### 1. Discretization and Solution Method

The states and controls are expanded based on Lagrange interpolating polynomials

$$\mathbf{x}^N(t) \approx \sum_{j=0}^N \mathbf{x}_j \phi_j(t), \quad \mathbf{u}^N(t) \approx \sum_{j=0}^N \mathbf{u}_j \phi_j(t) \quad (37)$$

The coefficients  $\mathbf{x}_j = \mathbf{x}(t_j)$ ,  $\mathbf{u}_j = \mathbf{u}(t_j)$  in Eq. (37) are the values of the states and controls at the Legendre-Gauss-Lobatto (LGL) points, which are the zeros of the derivative of the  $N$ th order Legendre polynomial  $L_N$  defined on the interval  $\tau \in [-1, 1]$ . The Lagrange interpolating polynomials are defined by

$$\phi_j(\tau) = \frac{(\tau^2 - 1) \dot{L}_N(\tau)}{(\tau - \tau_j) N(N+1) L_N(\tau_j)}, \quad j = 0, \dots, N \quad (38)$$

The state derivatives are approximated by analytically differentiating Eq. (37) and evaluating the result at the LGL points with the result expressible in terms of the differentiation matrix  $\mathbf{D}$ , whose components are defined by

$$D_{k,j} = \begin{cases} \frac{L_N(\tau_k)}{L_N(\tau_j)} \frac{1}{(\tau_k - \tau_j)} & k \neq j \\ -\frac{N(N+1)}{4} & k = j = 0 \\ \frac{N(N+1)}{4} & k = j = N \\ 0 & \text{otherwise} \end{cases} \quad (39)$$

The derivatives are easily expressed by the following relationship

$$\dot{\hat{\mathbf{x}}} \approx \frac{1}{\xi} \mathbf{D} \hat{\mathbf{x}} \quad (40)$$

where  $\hat{\mathbf{x}} \triangleq [\mathbf{x}_0, \dots, \mathbf{x}_N]$  is the discretized state vector across all nodes, and  $\xi$  is the transformation metric defined by the relationship between the computational domain  $\tau$  and the physical time domain  $t$

$$t = (t_j - t_0)\tau/2 + (t_0 + t_j)/2 \quad (41)$$

$$\xi \triangleq \frac{dt}{d\tau} = (t_j - t_0)/2 \quad (42)$$

Finally, the integral cost function is discretized via a Gauss-Lobatto quadrature rule so that

$$\int_{t_0}^{t_f} F(t) dt = \xi \int_{-1}^1 F(t(\tau)) d\tau \approx \xi \sum_{j=0}^N w_j F(t_j) \quad (43)$$

where  $w_j$  are the Legendre-Gauss-Lobatto weights defined by

$$w_j = \frac{2}{N(N+1)} \frac{1}{[L_N(\tau_j)]^2}, \quad k = 0, \dots, N \quad (44)$$

The process mentioned above is automated in the software DIDO, as well as in the software DIRECT written by the first author. This software is a MATLAB interface to the solver SNOPT, which implements a quasi-Newton algorithm.

## C. Numerical Results for Cross-Wind Motion

Previous work has established the importance of using cross-wind kite motion to generate large tension forces for power generation.<sup>29</sup> In this section, several different paths that move the kite across the wind ( $y$ -direction) are generated. In all cases, the period for the maneuver is fixed at 30 sec and the wind speed is nominally 10 m/s. Once a suitable reference trajectory is obtained, closed-loop simulations are conducted with unsteady winds. The wind

time history is similar to that shown in Fig. 9a, and is the same for all the simulation results shown in the following subsections. The kite properties are the same as those given in Table 1.

### 1. Case 1

In this example, the desired trajectory to be followed by the kite is given by

$$\bar{x}_h = 0, \quad \bar{y}_h = 20 \sin\left(\frac{2\pi t}{30}\right), \quad \bar{z}_h = 0 \quad (45)$$

which attempts to keep the kite within single plane. Note that this trajectory would be physically unrealizable, and hence the optimal control algorithm attempts to find the closest match to the trajectory while keeping the change in the attachment point position small. This is an example of an idealized reference trajectory – one that we desire the kite to move along, but which it is unlikely to, even in simulations. In addition, the reference trajectories could be specified in terms of the angle of the tether relative to the vertical position. However, for simplicity, the hinge point position is used as the reference for specifying the trajectories.

Closed-loop simulations with unsteady winds, together with the reference trajectories, are shown in Fig. 12. The time-varying trajectories are tracked extremely well, as shown in Fig. 12a. It can be seen that the kite is maintained reasonably close to  $x = 0$ , with a mean of -2 m, and a variation of approximately 1 m. The yaw angle of the kite, shown in Fig. 12b, illustrates that the kite changes heading by  $\pm 23$  deg. In other words, the kite points generally into the wind to generate most of its lift. The pitch of the plates varies by approximately 1 deg over the trajectory, whereas the roll of the plates varies by up to 6 deg. Fig. 12c shows that the reference variation in attachment point motion is very smooth, with a variation of approximately 5%. The two attachment points essentially move 180 deg out of phase with each other, which gives the optimal yaw and roll torques. The closed-loop trajectories show that the control input is never saturated, and that all variables are well-controlled.

### 2. Case 2

In this example, the desired trajectory to be followed by the kite is given by

$$\bar{x}_h = 0, \quad \bar{y}_h = 50 \sin\left(\frac{2\pi t}{30}\right), \quad \bar{z}_h = 50 \sin\left(\frac{4\pi t}{30}\right) \quad (46)$$

which attempts to fly a figure-of-eight in the vertical plane. Unfortunately, because the main tether is fixed in length, the variations in altitude to match the desired trajectory cannot be flown. This means that the idealized reference trajectory is also unlikely to be matched closely. Closed-loop simulations with unsteady winds, together with the reference trajectories, are shown in Fig. 13. The trace of the trajectory in the  $x$ - $y$  plane is shown in Fig. 13a, which shows that the trajectory is actually closer to a figure-of-eight in the horizontal plane. In this example, the velocity of the kite is larger than in the previous case, which means that the same changes in the wind speed have less impact on the motion. Hence, the tracking ability is increased. The yaw angle of the kite, shown in Fig. 13b, is substantially increased, with variations of  $\pm 100$  deg. The pitch of the plates shows high frequency variations, combined with sudden drops every half cycle. In other words, this trajectory is not as smooth as the previous one, but the tracking behavior is very good. The nominal variation in attachment point position is again shift 180 deg out of phase on each side of the kite. The closed-loop actuator inputs show some saturation for a limited time on rare occasions.

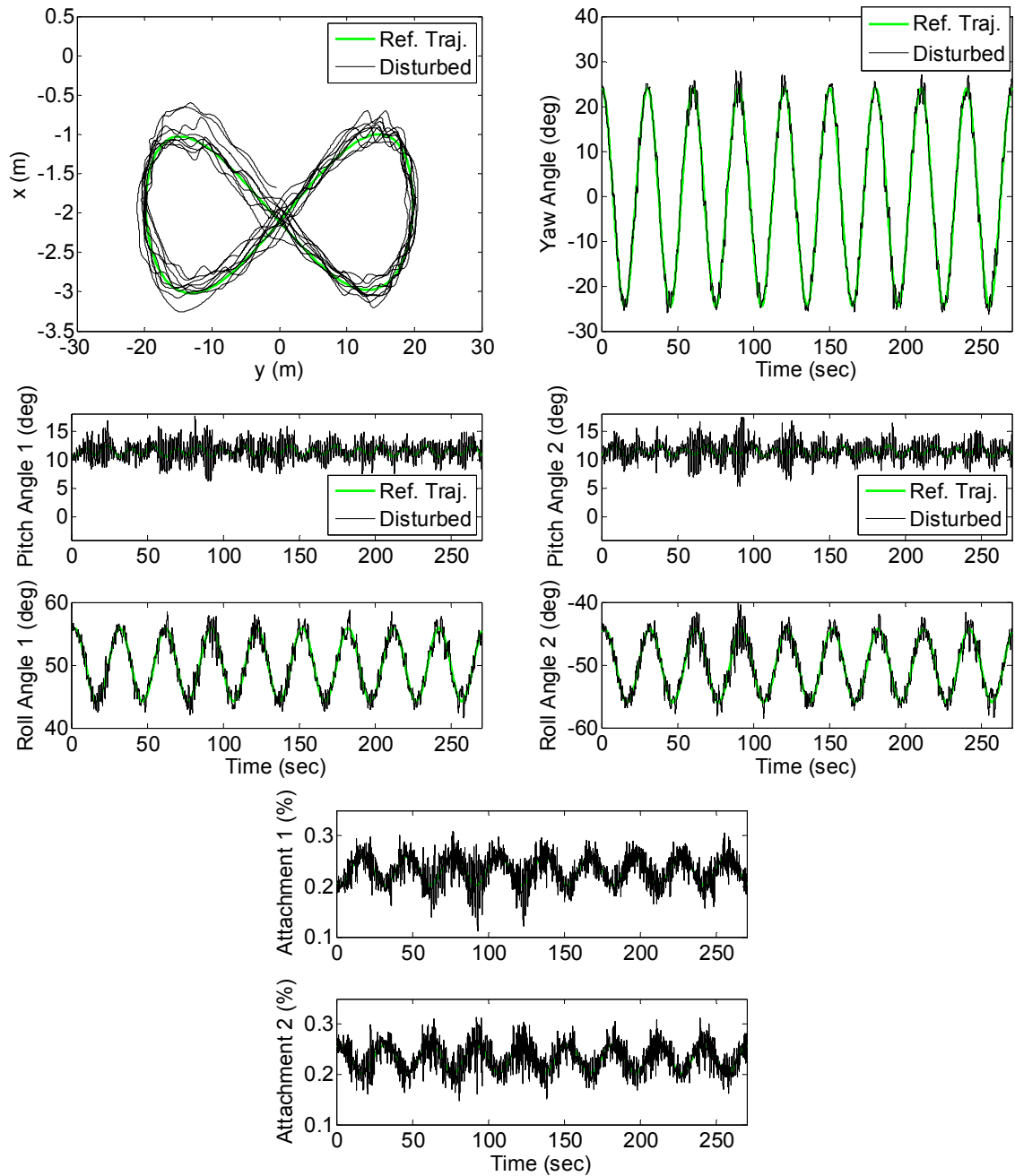


**Fig. 12** Closed-loop simulations of cross-wind kite motion, case 1: a) Hinge point position in x-y plane, b) Kite yaw angle, c) Pitch and roll of plate 1, d) Pitch and roll of plate 2, e) Attachment point positions.

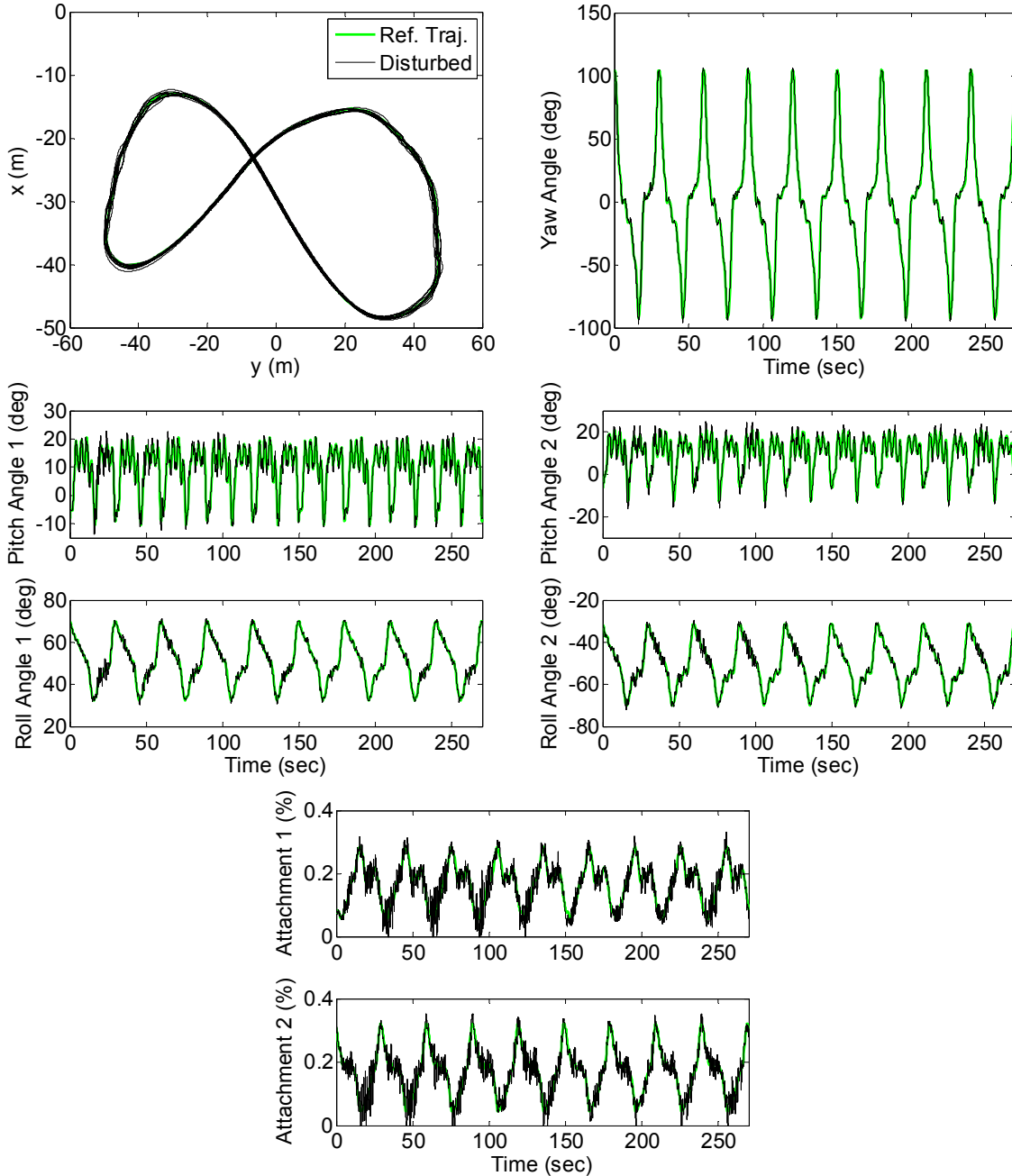


**Fig. 13** Closed-loop simulations of cross-wind kite motion, case 2: a) Hinge point position in x-y plane, b) Kite yaw angle, c) Pitch and roll of plate 1, d) Pitch and roll of plate 2, e) Attachment point positions.

### 3. Case 3

In this example, the desired trajectory to be followed by the kite is given by

$$\bar{x}_h = 20 \sin\left(\frac{2\pi t}{30}\right), \quad \bar{y}_h = 50 \sin\left(\frac{4\pi t}{30}\right), \quad \bar{z}_h = 0 \quad (47)$$

which attempts to fly a figure-of-eight in the horizontal plane, with the majority of the motion parallel to the wind direction. Closed-loop simulations with unsteady winds, together with the reference trajectories, are shown in Fig. 14. Fig. 14a shows that the reference trajectory of the kite approximates the figure-of-eight, but has a difficult time trying to maneuver with the wind due to the drop in relative wind speed. Therefore, the kite must fly more in the cross-wind direction to generate enough lift. This is reflected by the differences in the yaw angle of the kite, shown

in Fig. 14b. Tracking control of the kite position is achieved reasonably well. However, at approximately 150 sec, the attachment points saturate, which leads to some high frequency oscillations in the pitch, roll, and yaw of the kite.

#### 4. Case 4

In this final example, the desired trajectory to be followed by the kite is given by

$$\bar{x}_h = 50 \sin\left(\frac{4\pi t}{30}\right), \quad \bar{y}_h = 50 \sin\left(\frac{2\pi t}{30}\right), \quad \bar{z}_h = 0 \quad (48)$$

which attempts to fly a figure-of-eight in the horizontal plane, with the majority of the motion in the cross-wind direction. Closed-loop simulations with unsteady winds, together with the reference trajectories, are shown in Fig. 15. Fig. 15a shows that even in this case the idealized trajectories must be approximated by the kite. Although the shape of the trajectory is very close to a figure-of-eight, the amplitude of the  $x$ -component of the motion cannot be matched. The yaw angle of the kite, shown in Fig. 15b, varies by approximately  $\pm 45$  deg for the trajectory. The pitch of the plates show more substantial changes over the trajectory, peaking at about 25 deg. The plate roll angles vary by approximately 20 deg. Finally, the attachment point variation is the most extreme for this trajectory. In no case does the reference trajectory saturate on the lower bound, but the peak position is at close to half the chord of the kite. The results of Fig. 15 show the need to provide an adequate margin for feedback, since the actuators tend to saturate when the reference attachment point is close to its minimum. This has an obvious adverse effect on the dynamics. Hence, some improvements to the control algorithms will be necessary before the kite can be flown autonomously in a robust manner.

### V. Extension of Model to Multiple-Plates

The two-plate model is capable of being extended to the case where the kite is modeled by multiple plates. In such a case, it is necessary to utilize torsional springs to adequately couple the pitch and roll motions of each of the plates. A central hinge point is used at the center of the kite at the leading edge. An even number of plates are used so that the left and right wings of the kite are symmetric. The derivation of equations of motion can proceed using Lagrange's equations in the same fashion as presented earlier in this paper with additional terms for each plate. The inertial vector to the center of each plate must be used to calculate the inertial velocities. Additional potential energy terms must also be added to account for the effects of the torsional springs that constrain the relative pitch/roll angles between each plate.

To demonstrate the approach, consider the case where the kite is modeled using four plates. The parameters used to perform a simulation of the system are  $m_{\text{plate}} = 2.5$  kg,  $W = 2$  m,  $L = 5$  m. The spring stiffnesses for relative pitch are  $10^{-5}$  Nm/rad, and  $10^{-6}$  Nm/rad for relative roll between the plates. No spring stiffnesses are used at the centerline of the kite. The wind speed is 7 m/s, and all other parameters are the same as used previously. Numerical results are shown in Fig. 16 and Fig. 17. Fig. 16a shows the equilibrium position of the four-plate model. This shows that the center of the kite stays relatively straight compared to the elements closest to the attachment points. This is because lift dominates the forces at the center of the kite, whereas the side plates are dominated by the tether tension. This reflects the approximate shape of a real kite system, as shown in Fig. 1. Fig. 16b shows the results of a simulation with closed-loop control and unsteady winds. This illustrates that the system modeled with higher fidelity than the two-plate system can also be stabilized by movement of the attachment points. Fig. 17 shows the time histories of the key kite variables. The hinge point position is maintained very close to the zenith position. Disturbances of up to 2 m can be seen for the lateral position due to the peaks in the cross-wind velocity. The attachment point positions do not saturate, and require movements of up to 10 % from the equilibrium position.

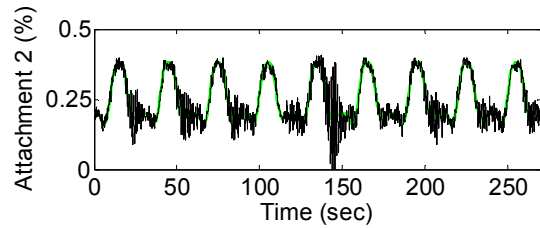
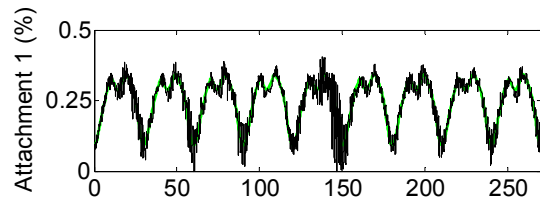
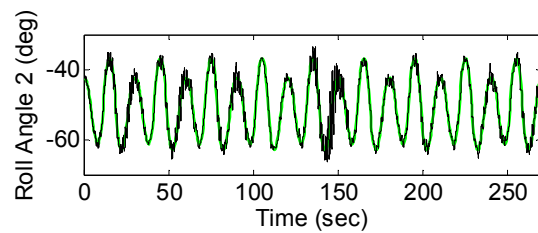
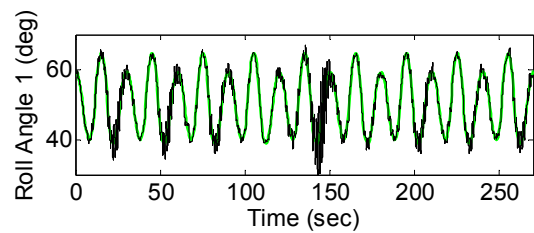
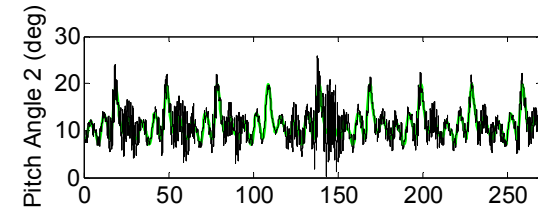
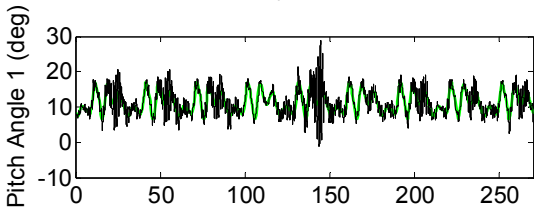
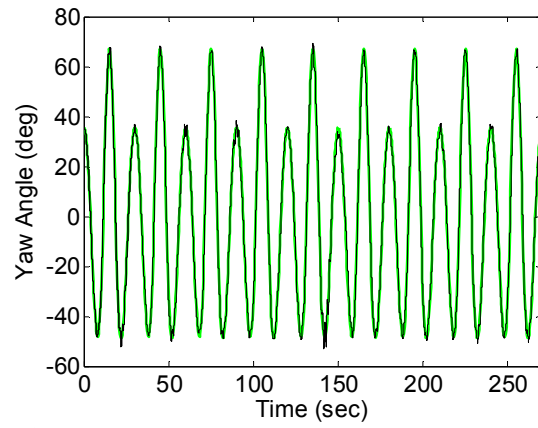
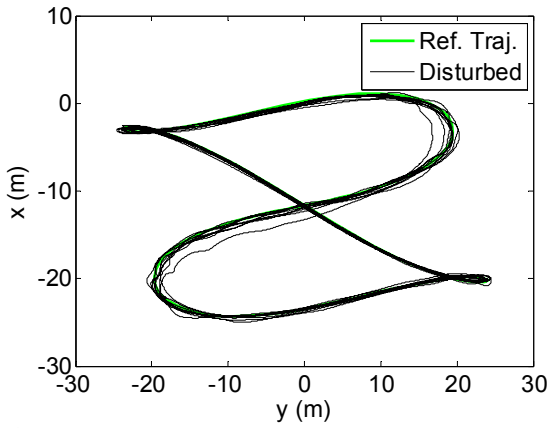


**Fig. 14** Closed-loop simulations of kite motion, case 3: a) Hinge point position in x-y plane, b) Kite yaw angle, c) Pitch and roll of plate 1, d) Pitch and roll of plate 2, e) Attachment point positions.

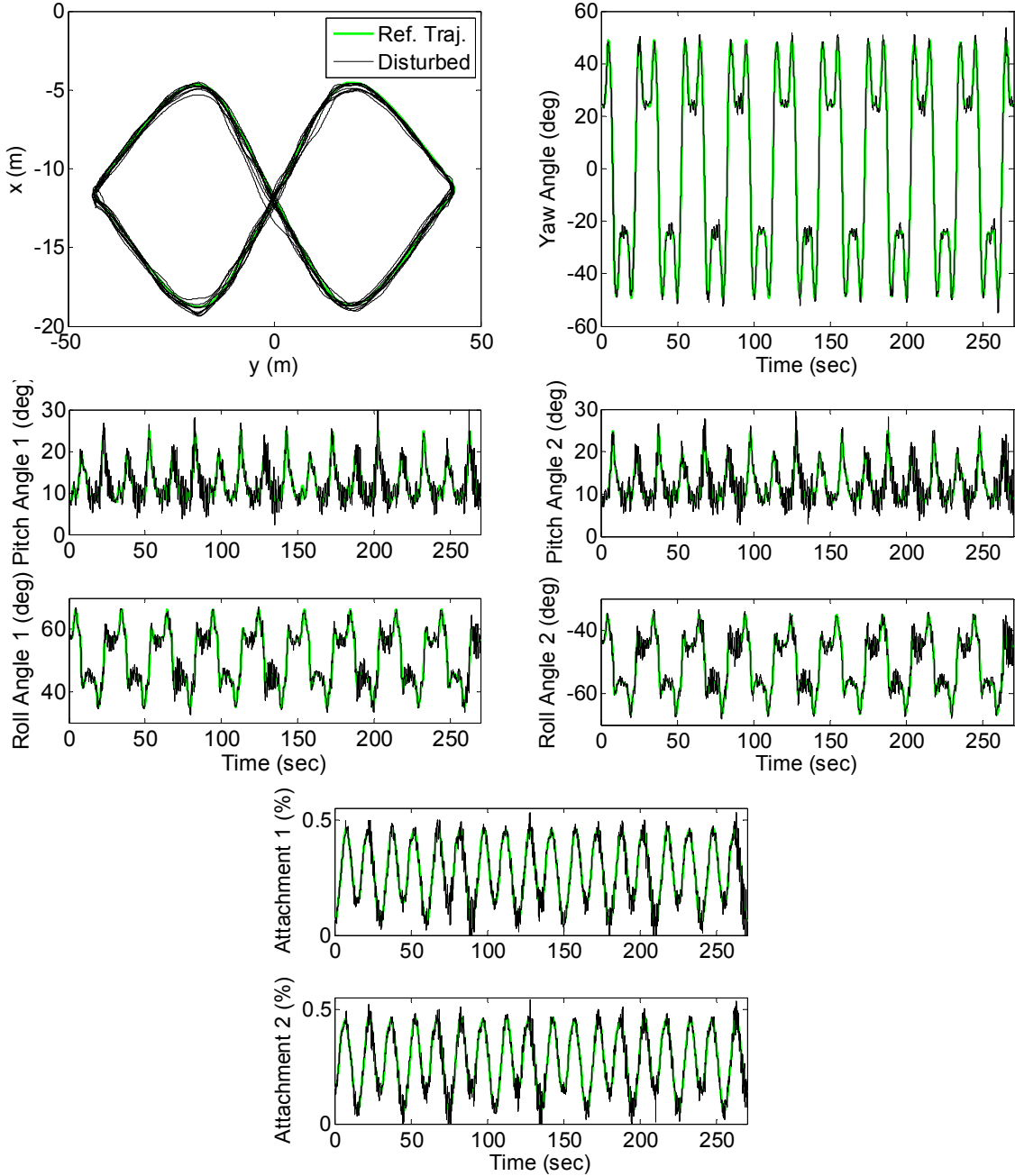


**Fig. 15** Closed-loop simulations of cross-wind kite motion, case 4: a) Hinge point position in x-y plane, b) Kite yaw angle, c) Pitch and roll of plate 1, d) Pitch and roll of plate 2, e) Attachment point positions.

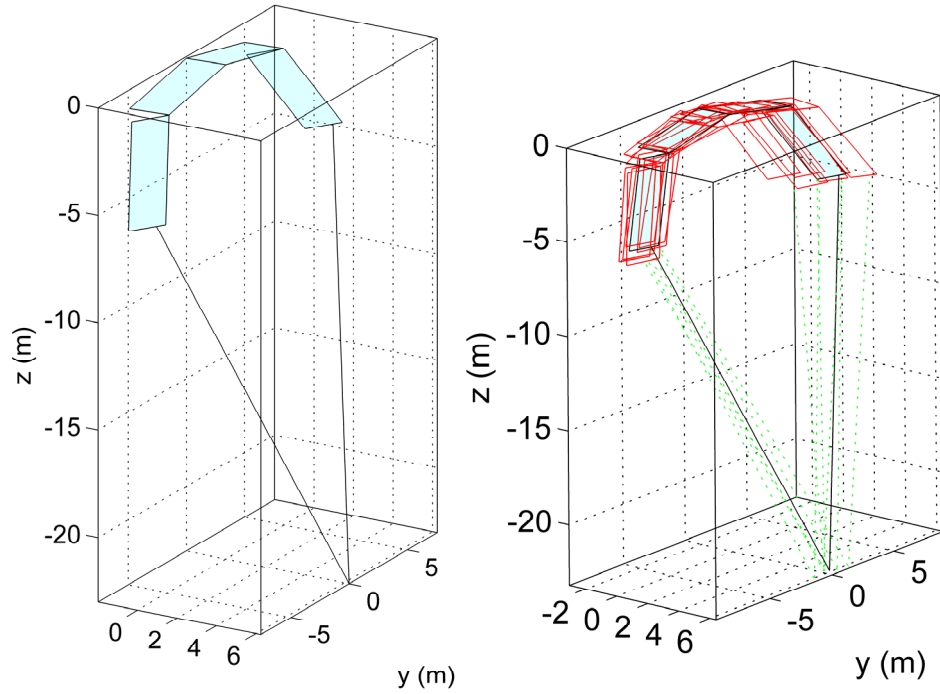


**Fig. 16** Four-plate kite model, a) Equilibrium position for 7 m/s wind, b) Closed-loop stationkeeping control in unsteady winds.

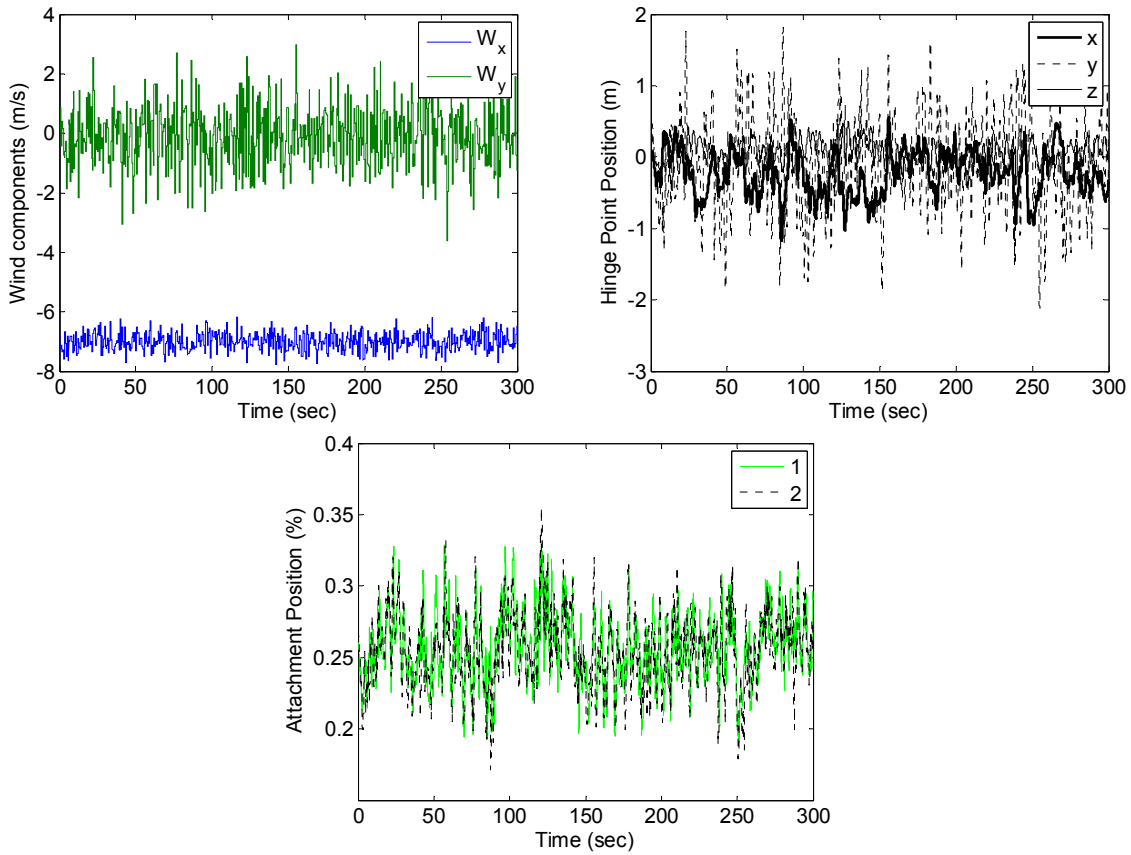


**Fig. 17** Simulation results for four-plate kite model in unsteady winds, a) Wind time history, b) Hinge point position, c) Attachment point position as fraction of chord.

## VI. Conclusions

A simplified representation of a flexible kite on a tether has been developed for approximating the motion and investigating aspects of control. A two-plate representation is able to capture the essential influence of movement of the tether attachment points for control. Kite control is based on simultaneously adjusting the tether attachment points so as to alter the pitch of each side of the kite, and hence, change the angle of attack. By judicious choice of control, rolling motion can also be induced to alter the tilt of the total lift vector. Stationkeeping control of the kite about a reference point proves to be relatively easy, whereas tracking time-varying trajectories is generally more difficult. This is largely the result of variations in the actuator inputs, which become more likely to saturate in the time-varying case. The two-plate model is easily extended to higher fidelity by using multiple plates. Control of a multiplate system can also be achieved using moveable attachment points. The ability to feedback dynamic states of the kite is dealt with in Part II, which implements a nonlinear dynamic observer for the system.

## References

- <sup>1</sup> Ockels, W.J., "Laddermill, a Novel Concept to Exploit the Energy in the Airspace," *Aircraft Design*, Vol. 4, 2001, pp.81-97.
- <sup>2</sup> Meijaard, J.P., Ockels, W.J., and Schwab, A.L., "Modelling of the Dynamic Behaviour of a Laddermill, A Novel Concept to Exploit Wind Energy," Proceedings of the Third International Symposium on Cable Dynamics, Norway, Aug. 1999, pp.229-234.
- <sup>3</sup> Lansdorp, B., and Ockels, W.J., "Comparison of Concepts for High-Altitude Wind Energy Generation with Ground Based Generator," Proceedings of the NRE 2005 Conference, Beijing, China, pp.409-417.
- <sup>4</sup> Lansdorp, B., Remes, B., and Ockels, W.J., "Design and Testing of a Remotely Controlled Surfkite for the Laddermill," World Wind Energy Conference, Melbourne, Australia, Nov. 2005.
- <sup>5</sup> Lansdorp, B., and Williams, P., "The Laddermill - Innovative Wind Energy from High Altitudes in Holland and Australia," Paper presented at Wind Power 2006, Adelaide, Australia, September 2006.
- <sup>6</sup> Carpenter, H.G., "Tethered Aircraft Having Remotely Controlled Angle of Attack," US Patent 5,931,416.
- <sup>7</sup> Carpenter, H.G., "Tethered Aircraft System for Gathering Energy From Wind," US Patent 6,254,034.
- <sup>8</sup> Roberts, B.W., and Shepard, D.H., "Unmanned Rotorcraft to Generate Electricity using Upper Atmospheric Winds," *Australian International Aerospace Congress*, Brisbane, July 2003.
- <sup>9</sup> Etkin, B., *Dynamics of Atmospheric Flight*, Wiley, New York, 1972.
- <sup>10</sup> Riegler, G., and Riedler, W., "Tethered Wind Systems for the Generation of Electricity," *Journal of Solar Energy Engineering*, Vol. 106, 1984, pp.177-181.
- <sup>11</sup> Riegler, G., Riedler, W., and Horvath, E., "Transformation of Wind Energy by a High-Altitude Power Plant," *Journal of Energy*, Vol. 7, No. 1, 1983, pp.92-94.
- <sup>12</sup> Fletcher, C.A.J., and Roberts, B.W., "Electricity Generation from Jet-Stream Winds," *Journal of Energy*, Vol. 3, 1979, pp.241-249.
- <sup>13</sup> Fletcher, C.A.J., "On the Rotary Wing Concept for Jet Stream Electricity Generation," *Journal of Energy*, Vol. 7, No. 1, 1983, pp.90-92.
- <sup>14</sup> Rye, D.C., "Longitudinal Stability of a Hovering, Tethered Rotorcraft," *Journal of Guidance, Control, and Dynamics*, Vol. 8, No. 6, 1985, pp.743-752.
- <sup>15</sup> Fry, C.M., and Hise, H.W., "Wind Driven, High Altitude Power Apparatus," US Patent 4,084,102, April 1978.
- <sup>16</sup> Kling, A., "Wind Driven Power Plant," US Patent 4,073,516, Feb. 1978.
- <sup>17</sup> Pugh, P.F., "Wind Generator Kite System," US Patent 4,486,669, Dec. 1984.
- <sup>18</sup> Biscomb, L.I., "Multiple Wind Turbine Tethered Airfoil Wind Energy Conversion System," US Patent 4,285,481, Aug. 1981.
- <sup>19</sup> Watson, W.K., "Airship-Floated Wind Turbine," US Patent 4,491,739, Jan. 1985.
- <sup>20</sup> Shepard, D.H., "Power Generation from High Altitude Winds," US Patent 4,659,940, April 1987.
- <sup>21</sup> Rundle, C.V., "Tethered Rotary Kite," US Patent 5,149,020, Sept. 1992.
- <sup>22</sup> Roberts, B.W., "Windmill Kite," US Patent 6,781,254, Aug. 2004.
- <sup>23</sup> Mouton, W.J., and Thompson, D.F., "Airship Power Turbine," US Patent 4,166,596, Sept. 1979.
- <sup>24</sup> Bolonkin, A., "Utilization of Wind Energy at High Altitude," AIAA Paper 2004-5705, Aug. 2004.
- <sup>25</sup> Loyd, M.L., "Crosswind Kite Power," *Journal of Energy*, Vol. 4, No. 3, 1980, pp.106-111.
- <sup>26</sup> Payne, P.R., and McCutchen, C., "Self-Erecting Windmill," US Patent 3,987,987, Oct. 1976.
- <sup>27</sup> Loeb, A., "Wind Driven Energy System," US Patent 4,124,182, Nov. 1978.
- <sup>28</sup> Lois, L., "Apparatus for Extracting Energy from Winds at Significant Height Above the Surface," US Patent 4,076,190, Feb. 1978.

<sup>29</sup>Williams, P., Lansdorp, B., and Ockels, W., "Optimal Cross-Wind Towing and Power Generation with Tethered Kites," submitted to AIAA Guidance, Navigation and Control Conference, Aug. 2007.

<sup>30</sup>Gill, P.E., Murray, W., and Saunders, M.A., "SNOPT: An SQP Algorithm for Large-Scale Constrained Optimization," *SIAM Journal on Optimization*, Vol. 12, No. 4, 2002, pp.979-1006.

<sup>31</sup>Williams, P., "Receding Horizon Control using Gauss-Lobatto Quadrature Approximations," *AAS/AIAA Astrodynamics Specialist Conference*, Aug. 7-11 2005, Embassy Suites Hotel, Lake Tahoe Resort, Paper AAS 05-349.

<sup>32</sup>Yan, H., Fahroo, F., and Ross, I.M., "Real-Time Computation of Neighboring Optimal Control Laws," AIAA Paper 2002-4657, Aug. 2002.

<sup>33</sup>Elnagar, J., Kazemi, M.A., and Razzaghi, M., "The Pseudospectral Legendre Method for Discretizing Optimal Control Problems," *IEEE Transactions on Automatic Control*, Vol. 40, No. 10, 1995, pp.1793-1796.

<sup>34</sup>Ross, I.M., and Fahroo, F., "Legendre Pseudospectral Approximations of Optimal Control Problems," *Lecture Notes in Control and Information Sciences*, Vol. 295, Springer-Verlag, New York, pp.327-342.